Thermal excitation effects of photoluminescence of annealed GaInNAs/GaAs quantum-well laser structures grown by plasma-assisted molecular-beam epitaxy

S. Z. Wang[a)]
Silicon Optoelectronics, Bio- and Nano-Systems Group, Corporate Technology R&D, STMicroelectronics, 5A Serangoon North Avenue 5, Singapore 554574

S. F. Yoon,[b)] W. J. Fan, and C. Y. Liu
School of Electrical and Electronic Engineering, Nanyang Technological University, Nanyang Avenue, Singapore 639798

S. Yuan
School of Materials Engineering, Nanyang Technological University, Nanyang Avenue, Singapore 639798

(Received 29 November 2004; accepted 18 April 2005; published 20 July 2005)

GaInNAs/GaAs quantum well laser structures have been grown by plasma-assisted molecular beam epitaxy. Rapid thermal annealing was applied to suppress the nitrogen-related localized states in the material. These nitrogen-related localized states significantly quench the photoluminescence due to its low radiative recombination efficiency, compared to band-to-band transitions. Further, the thermal excitation processes of carriers from localized states to extended states result in the high temperature-sensitivity of light emission, which may lead to a low characteristic temperature if such structures are used in a laser diode. Our experiments have shown that annealing at 760 °C for 120 s is insufficient to totally eliminate the nitrogen-related localized states, which may require a higher temperature anneal process. © *2005 American Vacuum Society.* [DOI: 10.1116/1.1935533]

I. INTRODUCTION

GaInNAs semiconductors and related quantum structures have recently attracted considerable attention due to their unique properties and promising applications for long-wavelength GaAs-based laser diodes in optical communication systems.[1,2] Quantum well active regions based on GaInNAs fabricated on GaAs substrate have shown lasing characteristics at 1.3 μm, which are comparable to results based on conventional InP technology.[3] Nevertheless, most 1.3 μm GaInNAs lasers exhibited lower characteristic temperature (T_0) coefficients than theoretically anticipated, with only marginal improvement in T_0 values over those achieved by conventional InP technology. Some recent works have attributed the lower than expected T_0 values in 1.3 μm GaInNAs lasers to large Auger recombination rates[4] in the material. Other works have indicated that the increase in carrier leakage and more temperature-sensitive gain are the key mechanisms, leading to the lower than expected T_0 values in 1.3 μm GaInNAs lasers.[5] So far, a comprehensive picture of the detailed mechanisms responsible for the temperature sensitivity of 1.3 μm GaInNAs lasers remains incomplete.

Temperature-dependent photoluminescence (PL) measurement is an important tool for studying the temperature sensitivity of semiconductor materials and related quantum structures.[6–8] Recently, a significant amount of PL data on GaInNAs have been reported, such as low-temperature, time-resolved, high pressure, and temperature-dependent characteristics.[9] All the above reports were largely related to the alloy disordering effect of as-grown nitrogen-containing alloys, leading to radiative recombination in localized centers at low temperature. No such localized recombination PL peak was observed in annealed samples. The temperature-dependent PL characteristic usually showed signs of progressive carrier detrapping from localized states to extended states. Only one very recent paper reported a twin PL structure of GaInNAs quantum well, related to transitions ($e1 \rightarrow \mathrm{hh1}, e1 \rightarrow \mathrm{lh1}$) between the first electron subband ($e1$) to the first heavy-hole (hh1) and light-hole (lh1) subband.[10] It did not relate the light- and heavy-hole energy splitting due to quantum confinement and strain effects to the temperature sensitivity of its optical property. Based on the current state of knowledge, many radiative mechanisms are unclear, and furthermore the intrinsic and extrinsic factors that affect the emission temperature sensitivity remain unknown.

In this paper, we report the growth procedure of GaInNAs/GaAs laser structures using solid source molecular beam epitaxy (SSMBE). Comparison of calculated energy levels of a strained GaInNAs/GaAs quantum well with measured PL peaks showed that only one PL peak originated from band-to-band transition, while the other PL peak was from localized state in the quantum well. Thermal excitation of carriers between these energy states (localized and ex-

[a)]The experimental part of this paper was finished at Microelectronics Center, School of Electrical and Electronic Engineering, Nanyang Technological University, Nanyang Avenue, Singapore 639798; electronic mail: shanzwang@yahoo.com
[b)]Author to whom correspondence should be addressed; electronic mail: esfyoon@ntu.edu.sg

TABLE I. "Laser Wafer" structure used in this work. The "Annealing Wafer" used in the annealing experiment had the same structure, except that the upper cladding layer was not grown.

Layer	Thickness (nm)	Doping ($1/cm^3$)	Growth temperature (°C)
GaAs	200	Be, 1×10^{19}	580
$Al_{0.4}Ga_{0.6}As$	1500	Be, 5×10^{17}	610
GaAs	150	undoped	580
$In_{0.35}Ga_{0.65}As_{0.983}N_{0.017}$	7	undoped	460
GaAs	150	undoped	580
$Al_{0.4}Ga_{0.6}As$	1500	Si, 5×10^{17}	610
GaAs	500	Si, 1×10^{18}	580
(100) GaAs substrate	400 micron	Si, 2×10^{10}	

tended) was investigated, and found to contribute to the temperature sensitivity of PL intensity following increase in temperature.

II. EXPERIMENTAL DETAILS

The GaInNAs laser structures were grown by radio frequency (rf) plasma-assisted solid-source molecular beam epitaxy. The growth chamber was equipped with standard effusion cells for group-III sources and cracker cells for group-V sources. The active nitrogen species were supplied using a rf nitrogen plasma source. The samples were grown on *n*-type (Si-doped) GaAs(001) substrates with carrier concentration of $\sim2\times10^{18}$ cm^{-3}. Prior to growth, surface oxide desorption was carried out under As flux at beam equivalent pressure (BEP) of 6.2×10^{-6} Torr. Streaky (2×4) surface reconstruction was maintained throughout the entire growth process. The BEPs for Ga and As were 4.5×10^{-7} and 6.2×10^{-6} Torr, respectively. The As/Ga flux ratio was fixed at ~14. The growth rate was ~1 μm/h, verified using time-resolved reflection high-energy electron diffraction (RHEED) measurements. The nitrogen rf plasma source worked optimally at nitrogen background pressure of 2.6×10^{-6} Torr and arsenic BEP_{As} of 6.2×10^{-6} Torr. To maintain the plasma in high brightness mode, the rf power is maintained greater than 60 W. Si and Be dopants were used for *n*-type and *p*-type doping of the expitaxial layers, respectively. Two wafers were grown under identical conditions. One was marked for laser fabrication (termed as "Laser Wafer"), while the other was marked for thermal anneal study (termed "Anneal Wafer"). The "Anneal Wafer" possessed identical structure as the "Laser Wafer," except the upper *p*-type cladding layer was not grown. Table I lists the layer information for these wafer samples.

After growth, a 200-nm-thick SiO_2 passivation layer was deposited. The "Anneal Wafer" was then diced into small pieces of 3 mm×3 mm prior to annealing. The samples were mounted at the center of a 4-in. Si wafer in the annealing chamber, which was purged with argon at 5 l/min for 5 min before the temperature was ramped up at a rate of 50 °C/s. The gas flow was then reduced and fixed at 2 l/min throughout the rest of the anneal process. The temperature variation was maintained within ±5 °C across the whole 4-in. Si wafer area.

PL measurements were performed using the 514.5 nm Ar-ion laser excitation line at near normal incidence. The PL signals were collected using a dual grating spectrometer in the reflection direction, and detected with a liquid-nitrogen cooled germanium (Ge) detector in association with a standard lock-in amplifier. For samples from the "Anneal Wafer," the anneal conditions were optimized based on PL measurements carried out at 77 K. These optimized conditions were then applied to samples from the "Laser Wafer," which were subjected to further temperature-dependent PL measurement.[11] These PL spectra were fitted with two Gaussian peaks to extract the energy positions and full-width at half-maximum value of the two peaks.

III. CALCULATION OF ENERGY LEVELS OF ANNEALED QUANTUM WELL

In terms of the PL characteristic, the direct effects of thermal anneal on a GaInNAs/GaAs quantum well are improvement in optical property, such as significant increase in PL intensity, reduction in PL linewidth, and blueshift (i.e., shift towards higher photon energy direction) of the PL peak.[12] Hence in most cases, thermal anneal is a desirable step in the device fabrication process. However, the mechanisms behind these anneal effects are complicated, reportedly including alloy disordering, suppression of nitrogen-related defects, In/Ga and N/As interdiffusion, well-width fluctuation, and nitrogen-related chemical bond reconfiguration.[13–15] Amongst these mechanisms, constituent atom interdiffusion across the quantum well interface stands out as an intrinsic physical mechanism, whereas other mechanisms can in practice be minimized by optimizing the material preparation technique. Hence, they are more commonly regarded as material-related mechanisms. There is substantial evidence in mature GaAs/AlGaAs, InGaAs/GaAs, and InGaAs/InP quantum structures that points to atomic interdiffusion across interfaces[16–18] as being one of the dominant effects from thermal anneal. Therefore in this work, the thermal anneal process will be treated as a key approach to fulfill constituent atomic interdiffusion.

A. Interdiffusion model

Many papers have reported the correlation between constituent In–Ga and N–As interdiffusion across GaInNAs/GaAs quantum well interfaces and the PL peak blueshift it entails. From PL results, some workers have deduced that in GaInNAs/GaAs quantum wells annealed at relatively low temperature (~650 °C), the interdiffusion process was dominated by In–Ga interdiffusion. However at higher temperature (~900 °C), N–As interdiffusion becomes dominant due to the large energy band bowing effect of GaAs-based nitrides.[19] Intuitively, both In–Ga and N–As interdiffusion should contribute to the PL blueshift in the anneal temperature range between 650 °C–900 °C. Recently, experimental evidence from composition-sensitive

high-resolution transmission electron microscopy measurements indicated that both In–Ga and N–As interdiffusion processes were present in samples annealed at 720 °C,[13] although the nitrogen diffusion coefficient ($D_{\mathrm{N-As}}$) is reportedly around three orders smaller[20] than the indium diffusion coefficient ($D_{\mathrm{In-Ga}}$).[21] Moreover, In and N diffusion coefficients vary with anneal temperature, and this will complicate the calculation of band structure of annealed GaInNAs/GaAs quantum wells. Hence, to simplify the calculation and taking into account results from Refs. 20 and 21, we assume the nitrogen diffusion length in our GaInNAs/GaAs quantum well samples annealed at 760 °C to be one-tenth of the indium diffusion length, i.e., $L_{\mathrm{In}} = 10L_{\mathrm{N}}$ ($L_d = \sqrt{Dt}$; t is the anneal time). For a GaInNAs/GaAs quantum well with as-grown indium and nitrogen mole fractions of x_0 and y_0, respectively, the indium and nitrogen composition profile (x,y) after anneal are given by[22]

$$x(z) = \frac{x_0}{2}\left[\mathrm{erf}\left(\frac{L_z + 2z}{4L_{\mathrm{In}}}\right) + \mathrm{erf}\left(\frac{L_z - 2z}{4L_{\mathrm{In}}}\right)\right], \tag{1a}$$

$$y(z) = \frac{y_0}{2}\left[\mathrm{erf}\left(\frac{L_z + 2z}{4L_{\mathrm{N}}}\right) + \mathrm{erf}\left(\frac{L_z - 2z}{4L_{\mathrm{N}}}\right)\right], \tag{1b}$$

where, L_z is the as-grown quantum well width. The coordinate position along the crystal growth direction is denoted by z, where $z=0$ at the center of the quantum well. L_{In} and L_{N} are the diffusion lengths of indium and nitrogen, respectively.

B. Energy gap of strained GaInNAs

The potential depth and shape of the GaInNAs/GaAs quantum well are determined by the indium and nitrogen composition. The compositional distribution function will finally determine the energy levels in the quantum wells. The ensuing diffusion process during annealing will smooth the potential depth and shape of the quantum well. In GaInNAs/GaAs quantum wells, one can expect this change to be significant because GaAs-based nitrides by far possess the largest energy-band bowing coefficient amongst most semiconductor alloys.[23,24] Because the nitrogen content in GaInNAs is usually less than 3%, most parameters, such as lattice constant in GaInNAs are deduced using linear interpolation between parameters of relevant binary semiconductors.[25] The energy gap (E_g) and effective mass (m_i with $i=e$, lh, and hh for electron, light hole, and heavy hole, respectively) of strained GaInNAs can be deduced using the following phenomenological relationships:[26]

$$E_g(\mathrm{Ga_{1-x}In_xN_yAs_{1-y}}) = E_g(\mathrm{Ga_{1-x}In_xAs}) - 69\ \mathrm{eV}\cdot\Delta e(x,y), \tag{2}$$

$$m_i(\mathrm{Ga_{1-x}In_xN_yAs_{1-y}}) = m_i(\mathrm{Ga_{1-x}In_xAs}) + 18.1667 m_0\cdot\Delta e(x,y), \tag{3}$$

where, $\Delta e(x,y) = e(x,y) - e(x,0)$ is the strain difference between $\mathrm{Ga_{1-x}In_xN_yAs_{1-y}}$ and $\mathrm{Ga_{1-x}In_xAs}$, while $e(x,y)$ $= [a(0,0) - a(x,y)]/a(x,y)$, where $a(x,y)$ is the lattice constant of $\mathrm{Ga_{1-x}In_xN_yAs_{1-y}}$.

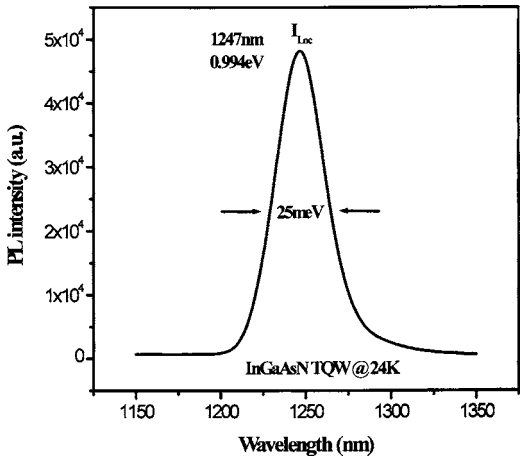

FIG. 1. PL spectrum obtained at 24 K from a 7-nm-width GaInNAs/GaAs quantum well sample annealed at 760 °C for 120 s.

C. Calculation of confined energy levels

It has been reported[26–28] that the band offset (ΔE_g) between GaInNAs quantum well and GaAs barrier follows the fraction $\Delta E_c : \Delta E_v = 70:30$, where ΔE_c and ΔE_v is the conduction and valence band discontinuity, respectively. Based on this, the 8-band k.p method is used to calculate the band structure of the GaInNAs/GaAs quantum well. The eigenfunctions $\phi(z)$ and corresponding energy levels E satisfy the following relationship:

$$[H_k(z) + U(z)]\phi(z) = E\phi(z), \tag{4}$$

where, $H_k(z)$ is the 8-band k.p Hamiltonian, and $U(z)$ the quantum well potential determined by Eqs. (1) and (2). Details of the 8-band k.p. approach have been published elsewhere.[29] In one of our previous papers,[11] it has been shown that with reference to electron and hole subband energy levels of as-grown and annealed GaInNAs/GaAs quantum wells, the calculation of the PL peak energy due to interband transitions can determine the diffusion length or diffusion coefficient in annealed samples. This takes into account the strain variation in the quantum well and carrier confinement layers due to In–Ga and N–As interdiffusion at different anneal temperatures. Hence based on this, it becomes possible to deduce the energy levels of as-grown and annealed GaInNAs/GaAs quantum wells using the diffusion lengths obtained in Ref. 11.

IV. RESULTS AND DISCUSSION

A. Temperature-dependent optical characteristics

Figure 1 shows the PL spectrum at 24 K of a 7-nm-thick $\mathrm{Ga_{0.65}In_{0.35}N_{0.017}As_{0.983}/GaAs}$ quantum well annealed at 760 °C for 120 s. The spectrum shows a Gaussian-shaped sharp PL peak at 0.994 eV (termed I_{Loc}) with linewidth (i.e., FWHM: full-width at half-maximum) of 25 meV. Figure 2 shows the PL spectrum at 50 K from the same sample with

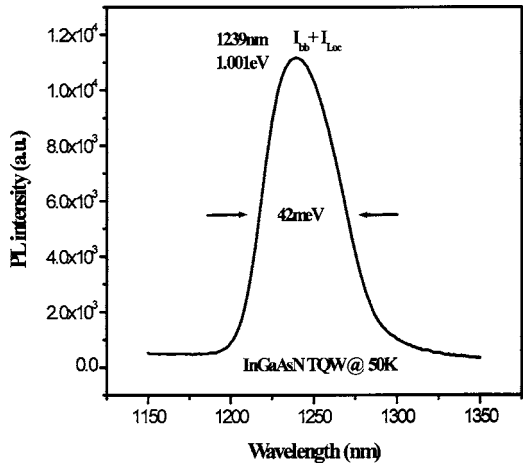

FIG. 2. PL spectrum obtained at 50 K from a 7-nm-width GaInNAs/GaAs quantum well sample annealed at 760 °C for 120 s.

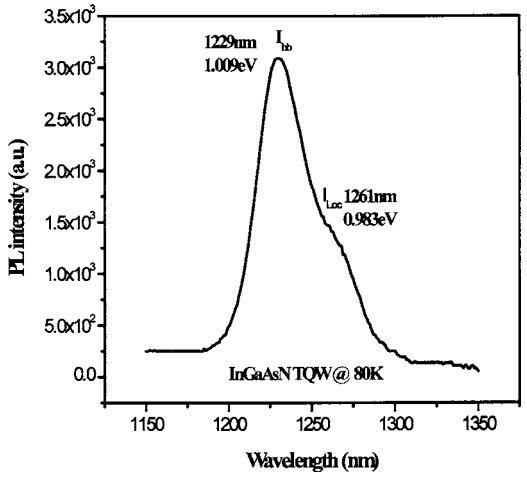

FIG. 4. PL spectrum obtained at 80 K from a 7-nm-width GaInNAs/GaAs quantum well sample annealed at 760 °C for 120 s.

the energy peak position at 1.001 eV (termed $I_{bb}+I_{\mathrm{Loc}}$) and a linewidth of 42 meV. Compared with the PL peak in Fig. 1, this PL peak possesses three characteristics. First, there is a blueshift in the PL peak energy from 0.994 eV to 1.001 eV that is not consistent with common knowledge that the energy gap of a semiconductor becomes smaller following increase in sample temperature.[7,8] Second, the PL spectrum broadens from 25 meV to 42 meV, an effect consistent with homogeneous broadening due to phonon scattering.[6] Third, the line shape of the PL spectrum exhibits an asymmetric characteristic with a low energy tail. Figure 3 shows the PL spectrum at 220 K from the same sample with the energy peak at 0.964 eV and linewidth of 35 meV (I_{bb} peak). Compared with Fig. 2, the PL peak energy redshifts from 1.001 eV to 0.964 eV at 220 K, in agreement with Varshni's relationship.[7,8] The PL linewidth narrows from 42 meV at 50 K to 35 meV at 220 K, which appears inconsistent with the homogeneous broadening effect from phonon scattering.[6] Furthermore, the PL spectrum reverts from its asymmetric characteristic at 50 K to symmetric characteristic at 220 K.

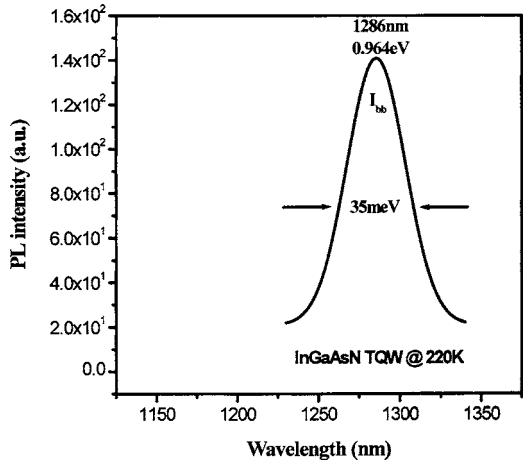

FIG. 3. PL spectrum obtained at 220 K from a 7-nm-width GaInNAs/GaAs quantum well sample annealed at 760 °C for 120 s.

When we pay attention to the PL spectra of this annealed $Ga_{0.65}In_{0.35}N_{0.017}As_{0.983}$/GaAs quantum well sample in the temperature range from 40 K to 200 K, we are even more curious to know what are the physical mechanisms that lie in behind the abovementioned temperature-dependent PL phenomena, because all the PL spectra in the temperature range from 40 K to 200 K (for example, 80 K in Fig. 4) reveal two emission peaks. Figure 4 shows the PL spectrum at 80 K from the same sample with one energy peak at 1.009 eV (I_{bb}) and a shoulder peak at 0.983 eV (I_{Loc}). Compared with the PL spectra at 24 K and 50 K, respectively, the I_{bb} peak (1.099 eV) is located at higher photon energy (blueshift) and the I_{loc} peak (0.983 eV) at lower photon energy (redshift). The PL intensity of the I_{bb} (1.009 eV) peak is stronger than that of the I_{Loc} (0.983 eV) peak. The convolution of these two PL peaks with each other will naturally lead to the complicacy of peak shifting, broadening and shaping properties of the annealed GaInNAs/GaAs quantum well sample.

B. Physical origins of PL peaks

To elucidate the physical mechanisms that contribute to the PL peak shift and spectrum broadening, the PL energy peak is plotted as a function of temperature as shown in Fig. 5. The open circles represent the data for the I_{Loc} PL peak, and the black squares represent the data for the I_{bb} PL peak. The solid and dashed curves are fitted results using Varshni's relationship[6]

$$E_g(T) = E_g(0) - \frac{\alpha T^2}{T+\beta} \tag{5}$$

with α=0.55 meV/K and β=3.05 K, respectively. The fitting yields two peak positions at 10 K of 0.9948 eV and 1.0178 eV, respectively, with an energy spacing of 23 meV. It is noted that there is only one PL peak when the sample temperature is lower than 40 K or higher than 200 K, as shown in Figs. 1 and 3. However, when the sample temperature lies between 60 K and 200 K, two distinguishable PL peaks are seen in the spectra, as shown in Fig. 4. This obser-

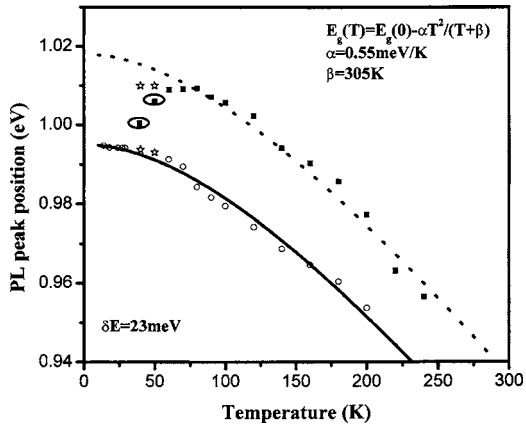

FIG. 5. PL peak positions from a 7-nm-width GaInNAs/GaAs quantum well sample annealed at 760 °C for 120 s as a function of measurement temperature.

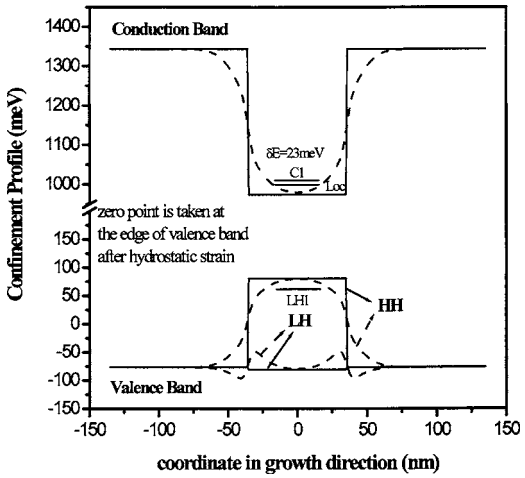

FIG. 6. Potential profiles for as-grown (solid) and annealed (dashed) GaInNAs/GaAs quantum well sample.

vation seems similar to results reported in Ref. 10, but with different physical origin of the PL peaks, as will be further discussed. Two special data points at 40 K and 50 K are observed, as indicated by two black squares surrounded by ovals in Fig. 5. The specialty is that there is only one broad PL peak (Fig. 2) while the peak position is in between the two fitting curves for different PL peaks (Fig. 5). We are ready to realize that at the temperatures from 40 K to 50 K there also exist two peaks in the PL spectrum but they convolute each other into one broad PL peak. Positioning in between the two individual peaks is a result of peak convolution. The deconvoluted results of the PL spectra acquired at 40 K and 50 K are presented in Fig. 5 as the star symbols, in accordance with the temperature-dependent trend.

Figure 6 shows the potential profiles of as-grown and annealed GaInNAs/GaAs quantum well samples. The solid lines indicate the potential profiles for electrons and holes, respectively, in the as-grown sample with 7-nm-thick $Ga_{0.65}In_{0.35}N_{0.017}As_{0.983}/GaAs$ quantum well. The dashed lines are potential profiles obtained using Eqs. (1)–(3) for electrons and holes, respectively, in the 7-nm-thick $Ga_{0.65}In_{0.35}N_{0.017}As_{0.983}/GaAs$ quantum well sample annealed at 760 °C for 120 s. The indium diffusion length is 1 nm and the nitrogen diffusion length is 0.1 nm.[11] The annealed sample has a smooth potential profile, which is quite different from that reported in Ref. 22, where only the indium diffusion effect is taken into account. The energy levels calculated using the 8-band k.p. approach for electrons and holes (both heavy and light) in the annealed $Ga_{0.65}In_{0.35}N_{0.017}As_{0.983}/GaAs$ quantum well sample are listed in Table II. Calculated results indicated the energy separation between hh1 and lh1 is around 90 meV. As this value is greater than the energy separation between the I_{bb} and I_{Loc} peaks in the PL spectrum of the annealed GaInNAs/GaAs quantum well sample, one may conclude that the twin PL peaks did not arise from the C1-hh1 and C1-lh1 transitions. Furthermore, it is unlikely that these two PL peaks both originate from band-to-band transitions, since the calculated energy separation between the sub-bands is not in agreement with the experimental energy separation between the two PL peaks. The calculated energy of the C1-to-hh1 transition at room temperature is in good agreement with the I_{bb} peak energy, indicating that the I_{bb} peak with higher energy arises from the C1-hh1 transition. The I_{Loc} energy peak is possibly from localized states at low temperature since the energy separation between the I_{bb} and I_{Loc} peaks did not agree with the calculated energy levels of the annealed quantum well sample.

C. Thermal excitation mechanisms

Figure 7 shows the temperature dependence of the integrated PL intensity for the annealed $Ga_{0.65}In_{0.35}N_{0.017}As_{0.983}/GaAs$ quantum well sample. The black squares denote the experimental data, and the solid and dashed curves correspond to the calculated results. The integrated PL intensity from the annealed $Ga_{0.65}In_{0.35}N_{0.017}As_{0.983}/GaAs$ quantum well sample decreases following an increase in sample temperature, sug-

TABLE II. Calculated energy levels for electron and hold in GaInNAs/GaAs quantum well annealed at 760 °C for 120 s. lh1 denotes the first subband of the light hole, hh1, hh2, and hh3 denote the first, second, and third subband of the heavy hole, and C1, C2, C3, and C4 denote the first, second, third, and fourth subband of the electron, respectively.

L_{In}(nm)	L_{N}(nm)	lh1(eV)	hh3(eV)	hh2(eV)	hh1(eV)	C1(eV)	C2(eV)	C3(eV)	C4(eV)
1	0.1	−49.249	−46.191	11.053	59.058	1000.806	1050.847	1123.238	1209.524
1	0.4	−50.046	−46.467	10.189	58.754	1001.01	1052.065	1125.086	1208.835
1	0.6	−51.017	−46.501	9.054	58.243	1001.564	1053.985	1126.943	1207.491

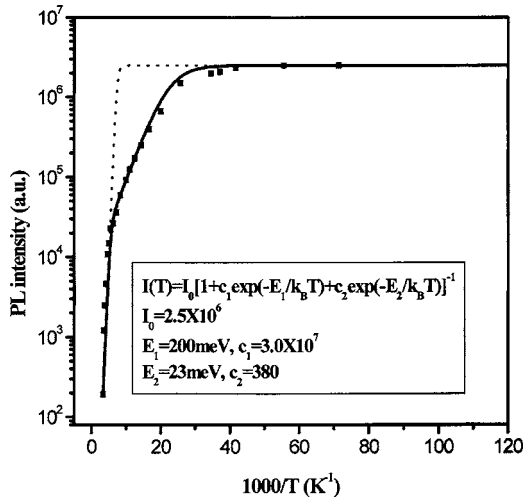

FIG. 7. Integrated PL peak intensity from a 7-nm-width GaInNAs/GaAs quantum well sample annealed at 760 °C for 120 s as a function of sample temperature.

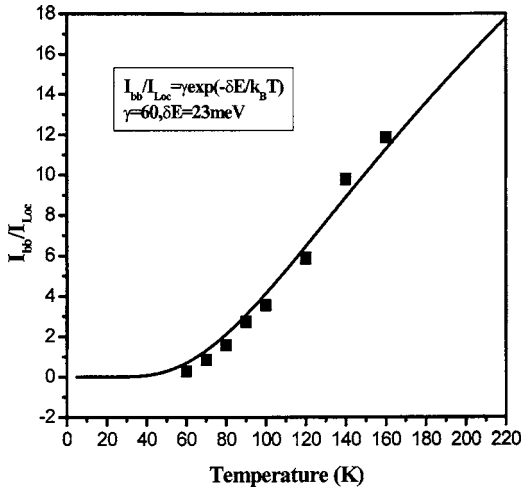

FIG. 8. PL peak intensity ratio from a 7-nm-width GaInNAs/GaAs quantum well sample annealed at 760 °C for 120 s drawn as a function of sample temperature.

gesting the presence of nonradiative recombination mechanisms. The data shows a clear temperature-dependent behavior characterized by two temperature regimes, corresponding to two thermally activated nonradiative mechanisms. The solid curve is the best fit to the experimental data following Eq. (6) below, which involves two nonradiative recombination processes:

$$I(T) = I_0[1 + C_1 \exp(-E_1/k_BT) + C_2 \exp(-E_2/k_BT)]^{-1}, \quad (6)$$

where 1 and 2 denote the two nonradiative mechanisms, respectively. I_0, C_1, and C_2 are constants. E_1 and E_2 are thermal activation energies corresponding to the respective nonradiative mechanisms, respectively. k_B is Boltzmann's constant, and T is the sample temperature. The best fit yields values of C_1 and C_2 of 3.0×10^7 and 380, and activation energies E_1 and E_2 of 200 meV and 23 meV, respectively. The dashed curve is the best fit to the experimental data considering the presence of one nonradiative mechanism by taking C_2 as zero in Eq. (6). The experimental data above 180 K could be explained within the framework of a one nonradiative mechanism model with activation energy E_1 of ~200 meV. The deviation of the one nonradiative mechanism model from experimental data at moderately low temperatures (<180 K) could be attributed to the presence of another nonradiative mechanism with activation energy E_2 of ~23 meV. It is noted that the value of E_2 is in good agreement with the energy spacing obtained in Fig. 5. This indicates that the decrease in integrated PL intensity at moderately low temperatures is attributed to the thermal activation of localized excitons to free excitons. The slight decrease (weighted by C_2=380 compared with $C_1=3.0\times10^7$) is the extrinsic property of the sample, which is determined by the defect characteristics such as its density. The physical origin of activation energy E_1 is currently unclear, and warrants further investigation.

The integrated PL intensity ratio of the I_{bb} peak over the I_{Loc} peak is plotted in Fig. 8 as a function of sample temperature. The black squares denote the experimental data, and the solid curve is the calculated fitting result. We consider an optical system comprising two energy levels at E_{bb} and E_{Loc}, respectively, with energy spacing $\delta E = E_{bb} - E_{\mathrm{Loc}}$ of 23 meV. Supposing the total generation rate of photogenerated carriers by laser excitation is N_0, the numbers of photogenerated carriers arriving at E_{bb} and E_{Loc} levels per unit time are

$$N_{bb} = N_0 \exp(-E_{bb}/k_BT), \quad (7)$$

$$N_{\mathrm{Loc}} = N_0 \exp(-E_{\mathrm{Loc}}/k_BT). \quad (8)$$

Because the luminescence intensity is proportional to the number of energy levels occupied, therefore,

$$I_{\mathrm{PL}(bb)} = k_{bb}N_{bb} = k_{bb}N_0 \exp(-E_{bb}/k_BT), \quad (9)$$

$$I_{\mathrm{PL(Loc)}} = k_{\mathrm{Loc}}N_{\mathrm{Loc}} = k_{\mathrm{Loc}}N_0 \exp(-E_{bb}/k_BT), \quad (10)$$

where, k_{bb} and k_{Loc} is the radiative recombination efficiencies for the E_{bb} and E_{Loc} levels, respectively. Hence, the integrated PL intensity ratio of the I_{bb} peak over the I_{Loc} peak is

$$I_{\mathrm{PL}(bb)}/I_{\mathrm{PL(Loc)}} = \gamma \exp(-\delta E/k_BT), \quad (11)$$

$$\gamma = k_{bb}/k_{\mathrm{ex}}, \quad \delta E = E_{bb} - E_{\mathrm{Loc}}, \quad (12)$$

where γ is defined as the radiative recombination efficiency ratio of the E_{bb} level over the E_{Loc} level, and remains the only fitting parameter in Eq. (11). The solid curve is the best fit of Eq. (11) to the experimental data. The fitting yields γ =60. The good agreement between the calculated result and experimental data indicates that the above theoretical deduction based on Boltzmann's distribution is reasonable. The result of γ=60 indicates that the radiative recombination efficiency for the E_{bb} level is much higher than that of the E_{Loc} level. This is reasonable considering the E_{Loc} level is merely a defect-related energy level whose radiative recombination efficiency is lower than that of band-to-band transitions. E_{loc}

could be an energy level caused by impurities, crystalline defects (such as nitrogen-related defects or indium-related defects), uniformity of material in the quantum well, and fluctuation of the quantum well width. Improvement in growth conditions will help to minimize the effects from well-width fluctuation, material uniformity and crystalline defects. Postgrowth annealing could also suppress the effect from crystalline defects and material uniformity. Furthermore, using source materials of high purity will help to minimize the presence of impurities in the sample.

The good agreement between the calculated data and experimental data over the entire temperature range concerned sheds light into the kinetic nature of the entire temperature-dependent process. Following increase in sample temperature, the carrier transfer process is fulfilled through three paths, viz., (i) carriers at the E_{bb} level are thermally activated to the conduction band of the GaAs barrier; (ii) carriers at the E_{Loc} level are thermally activated to the conduction band of the GaAs barrier; and (iii) carriers at the E_{Loc} level are thermally activated to the E_{bb} level. The energy spacing between the E_{bb} and E_{Loc} levels is only 23 meV. This value is much smaller ($\sim$10 times smaller) than the energy separation between the E_{bb} level or E_{Loc} level and conduction band of the GaAs barrier. Hence for simplicity, the thermal activation process between the E_{bb} or E_{Loc} level and conduction band of the GaAs barrier is not considered. Following increase in sample temperature, the carriers at the E_{Loc} level are thermally activated to the E_{bb} level. This decreases the carrier population at the E_{Loc} level and increases the carrier population at the E_{bb} level. Thus, the integrated PL intensity of the I_{Loc} peak is decreased and the integrated PL intensity of the I_{bb} peak is increased. The energy levels in annealed GaInNAs/GaAs quantum well are indicated in Fig. 6 as C1 (the first subband of the electron), lh1 (the first subband of the light hole), and Loc (the localized state of the electron), respectively.

It is worth noting that the localized energy level, though good for extension to longer wavelength, quenches the PL intensity rapidly. This could possibly result in poor characteristic temperature (T_0) in the laser diodes. The localized state is not intrinsic in the GaInNAs/GaAs quantum well and stands a good chance to be minimized by optimizing the growth process and postgrowth thermal anneal process. The elicitation from this work is that to keep the working energy level as far as possible from the other energy levels is guidance to design of high T_0 laser diodes.

V. CONCLUSIONS

Nitrogen-related localized states are known to form in GaInNAs/GaAs quantum wells during growth. At low temperature, such states exhibit emission at long wavelength due to thermal excitation of carriers from localized states to continuous states. Increase in temperature causes significant decrease in the PL intensity. A comparison between experimental results and calculated results shows that thermal annealing at 760 °C for 120 s was insufficient to totally eliminate the nitrogen-related localized states. The radiative recombination efficiency of carriers at such localized states is around 60 times lower than that of carriers at continuous states, indicating that the nitrogen-related localized states behave as nonradiative recombination centers. Further investigation is necessary to find suitable process conditions to eliminate such nitrogen-related localized states in the GaInNAs material.

ACKNOWLEDGMENTS

The authors are grateful to S.Y.Xie, Y.X.Dang, and Y.Qu for technical assistance.

[1] M. Kondow, T. Kitatani, K. Nakahara, and T. Tanaka, Jpn. J. Appl. Phys., Part 1 **38**, 1355 (1999).
[2] M. Fischer, M. Reinhardt, and A. Forchel, Electron. Lett. **36**, 1208 (2000).
[3] D. A. Livshits, A. Yu. Egorov, and H. Riechert, Electron. Lett. **36**, 1381 (2000).
[4] R. Fehse, S. Jin, S. J. Sweeney, A. R. Adams, E. P. O'Reilly, S. Illek, A. Yu. Egorov, and H. Riechert, Proc. IEEE **1**, 330 (2001).
[5] N. Tansu and L. J. Mawst, IEEE Photonics Technol. Lett. **14**, 1052 (2002).
[6] S. Z. Wang, S. F. Yoon, L. He, and X. C. Shen, J. Appl. Phys. **90**, 2314 (2001).
[7] S. Z. Wang and S. F. Yoon, J. Appl. Phys. **91**, 5066 (2002).
[8] S. Z. Wang and S. F. Yoon, J. Appl. Phys. **93**, 5091 (2003).
[9] S. Shirakata, M. Kondow, and T. Kitatani, Appl. Phys. Lett. **80**, 2087 (2002), and reference therein.
[10] N. J. Kim, Y. D. Jang, D. Lee, K. H. Park, W. G. Jeong, and J. W. Jang, Appl. Phys. Lett. **83**, 3114 (2003).
[11] Y. Qu, C. Y. Liu, S. Yuan, S. Z. Wang, S. F. Yoon, Micheel C. Chan, and M. H. Hong, J. Appl. Phys. **95**, 3422 (2004).
[12] S. Z. Wang, S. F. Yoon, T. K. Ng, W. K. Loke, and W. J. Fan, J. Cryst. Growth **242**, 87 (2002).
[13] M. Albrecht, V. Grillo, T. Remmele, H. P. Strunk, A. Yu. Egorov, Gh. Dumitras, H. Riechert, A. Kaschner, R. Heitz, and A. Hoffmann, Appl. Phys. Lett. **81**, 2719 (2002).
[14] W. Chang, J. Lin, W. Zhou, S. J. Chua, and Z. C. Feng, Appl. Phys. Lett. **79**, 4497 (2001).
[15] S. Z. Wang, S. F. Yoon, W. K. Loke, C. Y. Liu, and S. Yuan, J. Cryst. Growth **255**, 258 (2003).
[16] L. V. Dao, M. B. Johnston, M. Gal, L. Fu, H. H. Tan, and C. Jagadish, Appl. Phys. Lett. **73**, 3408 (1998).
[17] P. G. Piva, S. Charbonneau, I. V. Mitchell, R. D. Goldberg, Appl. Phys. Lett. **68**, 2252 (1996).
[18] K. Kerkel, J. Oshinowo, A. Forchel, J. Weber, and E. Zielinski, Appl. Phys. Lett. **76**, 3456 (1995).
[19] Z. Pan, L. H. Li, W. Zhang, Y. W. Lin, R. H. Wu, and W. Ge, Appl. Phys. Lett. **77**, 1280 (2000).
[20] L. H. Li, Z. Pan, W. Zhang, Y. W. Lin, Z. Q. Zhou, and R. H. Wu, J. Appl. Phys. **87**, 245 (2000).
[21] S. Burkner, M. Baeumler, J. Wagner, E. C. Larkins, W. Rothemund, and J. D. Ralston, J. Appl. Phys. **79**, 6818 (1996).
[22] M. C. Y. Chan, C. Surya, and P. K. A. Wai, J. Appl. Phys. **90**, 197 (2001).
[23] W. G. Bi and C. W. Tu, Appl. Phys. Lett. **70**, 1608 (1997).
[24] A. Yu. Egorov, D. Bernklau, B. Borchert, S. Illek, D. Livshits, A. Rucki, M. Schuster, A. Kaschner, A. Hoffmann, Gh. Dumitras, M. C. Amann, and H. Riechert, J. Cryst. Growth **227–228**, 545 (2001).
[25] S. L. Chuang, *Physics of Optoelectronic Devices* (Wiley, New York, 1995), p. 709, and references therein.
[26] W. W. Chow, E. D. Jones, N. A. Modine, A. A. Allerman, and S. R. Kurtz, Appl. Phys. Lett. **75**, 2891 (1999).
[27] W. J. Fan and S. F. Yoon, J. Appl. Phys. **90**, 843 (2001).
[28] M. Kondow, T. Kitatani, S. Nakatsuka, M. Larson, K. Nakahara, Y. Yazawa, M. Okai, and K. Uomi, IEEE J. Sel. Top. Quantum Electron. **3**, 719 (1997).
[29] J. Los, A. Fasolino, and A. Gatellani, Phys. Rev. B **53**, 4630 (1996).